MSANTD3 is a novel high expressed gene in HNSCC metastasis and interferes with cell migration

Shuzhou Liu (shuzhou_liu@yeah.net)
Hainan General Hospital, Hainan Affiliated Hospital of Hainan Medical University
Yuliang Zhang
Hainan General Hospital, Hainan Affiliated Hospital of Hainan Medical University
Anyan Zhou
Hainan General Hospital, Hainan Affiliated Hospital of Hainan Medical University
Jing Zheng
Hainan General Hospital, Hainan Affiliated Hospital of Hainan Medical University
Jiabin Nian
Hainan General Hospital, Hainan Affiliated Hospital of Hainan Medical University

Research Article

Keywords: C9orf30, TCGA, survival, YD-15, BICR-56

Posted Date: April 12th, 2022

DOI: https://doi.org/10.21203/rs.3.rs-1526750/v1

Abstract

Background Head and neck squamous cell carcinoma (HNSCC) is one of the most common cancer in the world. This study proposed MSANTD3 as a prognostic biomarker for HNSCC and a regulator for cancer cell migration.

Methods We analyzed the expression and survival association of MSANTD3 in HNSCC using open data. We compared the expression of MSANTD3 in tumors from primary and metastasis HNSCC tissues using QPCR and western blotting. We determined the migration velocity of multiple HNSCC cell lines using a chemotaxis migration assay. We analyzed the correlation between MSANTD3 expression and HNSCC cell migration. We also test the effect of MSANTD3 knockdown and overexpression on HNSCC cell migration.

Results MSANTD3 was overexpressed in HNSCC than normal head and neck tissues and metastasis HNSCC than primary HNSCC. MSANTD3 expression was associated with significantly poorer overall survival of HNSCC patients. MSANTD3 level was correlated with the migration velocity in HNSCC cell lines. Knockdown of MSANTD3 reduced the migration and the overexpression of MSANTD3 promoted the migration of HNSCC cell line YD-15 and BICR-56.

Conclusion 1) MSANTD3 is higher expressed in HNSCC than normal tissue and in metastatic than primary tumor; 2) cells with high MSANTD3 presented higher migration velocity; 3) the overexpression and knockdown of MSANTD3 interfered on cell migration.

1. Introduction

Head and neck squamous cell carcinoma (HNSCC) is the sixth most common cancer in the world. Each year, there are more than eight hundred thousand new cases of HNSCCC around the world, and results in about three hundred thousand deaths worldwide [1]. Although surgical treatment, radiotherapy, and chemotherapy have been applied for the clinical treatment of HNSCC, currently, the prognosis of most HNSCC patients is unfavorable [2]. Recently, immunotherapy such as PD1 blocker was provided a novel approach for HNSCC treatment [3]. One of the most challenging issues in clinical HNSCC treatment is the difficulty in diagnostic and prognostics of the HNSCC. In most HNSCC cases, a late diagnosis and treatment of HNSCC can lead to cancer cell lymph node metastasis and result in a much higher death risk of patients [4]. Therefore, the study in biomarkers for HNSCC diagnostic and prognostic is urgent for the clinical treatment of HNSCC patients. Moreover, the study in potential HNSCC cell migration regulators for HNSCC is also key to the prevention and treatment of HNSCC metastasis.

Myb/SANT-Like DNA-Binding Domain-Containing Protein 3, MSANTD3, also called C9orf30, is a protein-coding gene associated with DNA-Binding. Although MSANTD3 in cancer has not been studied sufficiently, MSANTD3 was found to be potentially associated with some types of cancer [5] [6] [7] [8]. The recurrent rearrangements of MSANTD3 in salivary gland acinic cell carcinoma were identified as a recurrent event during disease pathogenesis [5]. The fusion of Histatin 3 (HTN3) and MSANTD3 gene was found to be critical in a subtype of acinic cell carcinoma of the salivary gland [9], inferring its potential roles in cancer in general. A recent study further demonstrated that MSANTD3 is one of the biomarkers of one of the subgroups of acinic cell carcinoma [6]. In addition, studies also revealed the potential of MSANTD3 as a prognostic biomarker. MSANTD3 was identified as one of the ten most significant prognostic marker genes differing between normal tissues and tumor tissues of breast cancer patients [7]. MSANTD3 was also identified as one of the six candidate genes that potentially affect therapeutic response in non-small cell lung cancer patients [8]. However, so far, no study has reported the role of MSANTD3 in HNSCC. So far, whether MSANTD3 is functionally critical in HNSCC has never been studied.

In this study, we investigated the expression of MSANTD3 in clinical HNSCC patients and HNSCC cell lines. We proposed that MSANTD3 might be a regulator for the migration of HNSCC cells. This study identified MSANTD3 as a potential prognostic biomarker for HNSCC with regulatory effects on HNSCC cell migration.

2. Methods

2.1. Bioinformatic analysis

The transcriptome data of HNSCC were downloaded from The Cancer Genome Atlas (TCGA) in January 2020, following the required guidelines and policies. R foundation for statistical computing (2020) version 4.0.3 and ggplot2 (v3.3.2) was used to conduced bioinformatic analysis. The Oncomine tools [10] were also used to access and analyze the expression and copy number data. Data set GSE25099 [11], GSE9844 [12], and GSE25103 [11] were analyzed. The protein-protein interaction network was constructed using the String [13].

2.2. The acquisition of clinical HNSCC samples

HNSCC tissue samples were collected from 32 patients between March 2021 and September 2021 in Hainan General Hospital. 16 primary HNSCC tissues and 16 HNSCC distant metastasis tissues were collected. All donors were older than 18 years old and have been informed and consented to the use of the samples. Basic patient characteristics were provided in the supplementary file.

2.3. Cell culture

All the cell lines were obtained commercially and the Cell line authentication was provided by the providers. HSC-3 (SCC193) was purchased from Sigma-Aldrich (Hertfordshire, UK). SNU-46 and YD-38 were provided by the Korean Cell Line Bank (Seoul, Korea). YD-15 was purchased from the Creative Bioarray (Shirley, NY, USA). BICR-16 (BIR-16), BICR-22, and BICR-6 were purchased from the ECACC (Salisbury, UK). BICR-56 were purchased from the DSMZ

(Braunschweig, Germany). All cells were cultured in DMEM + 2mM Glutamine + 10% Fetal Bovine Serum (FBS) in an incubator of 5% CO_2 and 37°C. The authentication of SNU-46

2.4. Cell transfection

MSANTD3 knockdown and overexpression were achieved by transfecting shRNA or expression plasmid into cells. The predesigned MSANTD3 shRNA (MSANTD3 Human shRNA Plasmid Kit Locus ID 91283) plasmid and Control (Lenti particles Scrambled shRNA), Human MSANTD3 expression plasmid (made from RC203850), and packaging plasmids Lenti-vpak packaging kit with transfection reagent (TR30037) were purchased from OriGene (Rockville, MD, USA) and the experiments followed the instruction of the kit.

2.5. QPCR

The mRNA levels of MSANTD3 in cell samples and tissue samples were determined using QPCR assay[14]. Briefly, RNA was obtained using the RNeasy Mini kit (Qiagen, Germantown, MD, USA). The PrimeScript RT Reagent kit with gDNA Eraser (Takara Bio, Japan) was used to conduct the retro transcription. The PowerUp™ SYBR™ Green Master Mix (Thermo, Beverly, MA, USA) was used to conduct the QPCR. The Applied Biosystems StepOnePlus instrument (Thermo, Beverly, MA, USA) was used to control the reaction temperature. The results were normalized using the 2-ΔΔCT method. The sequences of the primers were as follows: MSANTD3 forward: 5’- TCCAGCAGATAGAGCGAGAG-3’; MSANTD3 reverse: 5’- ATTACAAGAGAGCCACCCCC-3’; GAPDH forward 5' -ACAACTTTGGTATCGTGGAAGG-3'; GAPDH reverse: 5'-GCCATCACGCCACAGTTTC-3'.

2.6. Western blotting

The protein level of MSANTD3 in tissues and cell lines was determined using western blotting. Briefly, proteins in samples were isolated using the protein lysing buffer (Pierce, Rockford, IL, USA) with protease inhibitors (Roche, Indianapolis, IN, USA). The proteins were separated using 10–12% sodium dodecyl sulfate-polyacrylamide gels. The proteins were then transferred to nitrocellulose membranes (Pall Corporation, Port Washington, NY, USA). The membrane was blocked in the western blotting blocking buffer. Then the membranes were incubated with the primary antibodies overnight at 4°C and secondary antibodies at RT for 1 hour. ECL solution was used to visualize the protein on the membrane. The images were then quantified by ImageJ. Antibodies used for western were MSANTD3 Antibody (NBP1-98441), Anti-GAPDH antibody [6C5]-Loading Control (ab8245), and Rabbit Anti-Mouse IgG H&L (HRP) (ab6728).

2.7. Immunohistochemistry

Immunohistochemistry was used to visualize the protein expression in tissue samples. Paraffin-embedded tumor samples were deparaffinized in xylene, rehydrated through graded ethanols, and submerged into the citric acid buffer for heat-induced antigenic retrieval. The samples then were blocked with 10% BSA, following the incubation with the MSANTD3 Antibody (NBP2-57629) at 4°C overnight, and developed using the DAKO ChemMate Envision Kit HRP (Dako-Cytomation, Carpinteria, CA, USA) followed by counterstaining with hematoxylin, dehydration, clearing and mounting.

2.8. Chemotaxis assay

Real-time cell migration recording of individual cells was conducted using the m-Slide chemotaxis system (ibidi, Germany) [15, 16]. Briefly, cells were adhering on the central channel of the chemotaxis slide at 10–20% confluency. A time-lapse Micro-Imager and computer were used to record the images of cells for 10 hours. The tracks of the individual cell were recoded, and the velocity of cell migration was analyzed using the Ibidi software.

2.9. Repetition and statistics analysis

The survival data were analyzed using the Kaplan-Meier (KM) and the Cox regression analysis. The KM analysis used a fixed cutoff of 50% (comparing 50% high expression samples with 50% low expression samples). The Cox regression analysis, also called proportional hazards regression, was conducted for investigating the effect of several variables, including MSANTD3 expression, on patient survival, assuming that the effects of the predictor variables on survival are constant over time and are additive in one scale. Western Blotting (WB), q-PCR, and chemotaxis assays were performed in triplicates with at least 5 biological replicates. Experimental data were presented in means ± standard deviations in the bar charts. A t-test or ANOVA was used to assess the significance ($p < 0.05$). Dunnett’s post hoc tests were used to test the difference between groups. The GraphPad Prism (version 8) was used to calculate statistics.

3. Results

3.1. MSANTD3 is overexpressed in HNSCC.

This study explored the clinical value of MSANTD3 as a biomarker for HNSCC. We first compared the MSANTD3 level HNSCC transcriptome and head and neck normal tissues. Results showed that MSANTD3 was significantly overexpressed in HNSCC compared to paired normal tissues in TCGA (Fig. 1A). We also compared HNSCC and adjacent normal tissues in the same patient and did a paired analysis. Results showed that all HNSCC expressed higher adjacent normal tissues (Fig. 1B). Based on the TCGA data, we plotted the receiver operating characteristic (ROC) curve for the higher expression of MSANTD3 in the HNSCC. Results showed that the area under the curve (AUC) was 0.959 (95%CI = 0.940–0.979), indicating that MSANTD3 is a highly expressed gene in HNSCC (Fig. 1C). In addition, we also used two external data sets to validate the high expression of MSANTD3. Results showed that MSANTD3 was overexpressed in HNSCC compared to normal tissues in both Peng’s data (GSE25099) [11] and Ye’s data (GSE9844) [12] (Fig. 1D-E). We also found that the copy number of MSANTD3 in HNSCC was significantly higher than that in normal head and neck tissues (Fig. 1F-G). These data suggested that the higher expression of MSANTD3 might result from the higher copy number in cancer tissue.

3.2. MSANTD3 is a potential prognostic biomarker for HNSCC.

In this study, we also explored the prognostic value of MSANTD3 for HNSCC. We analyzed the potential association of MSANTD3 expression and the overall survival of HNSCC patients using TCGA cohort. Detailed patient characteristics in the MSANTD3 high group and MSANTD3 low group (50%) were shown in Table 1. Based on a single risk factor MSANTD3 expression level, we plotted the dotted line of all HNSCC patients and divided the patients into high and low-risk groups. The analysis used a fixed cutoff of 50% (comparing 50% high expression samples with 50% low expression samples). There are 250 samples in the high group and 251 samples in the low group (Fig. 2A top panel). The survival status (censored alive or dead events) and censored time points of the patients were plotted in the middle panel, vertically corresponding to the expression z-score (Standard score) heatmap of the MSANTD3 at the bottom panel. The x-axis was the z-score of sample MSANTD3 expression (Fig. 2A). Results showed that in the high-risk groups (left part of the panel), points were clustered at shorter censored time points, while in the low-risk groups (right part of the panel), points were scattered to a longer survival time (Fig. 2 middle). The Kaplan-Meier overall survival analysis log-rank test comparing the survival of the high and low-risk groups revealed that the high MSANTD3 group (50–100%) had a significantly higher overall survival rate than the low MSANTD3 group (0–50%). The hazard ratio of the high group calculated by Cox regression was 1.811 (95%CI = 1.38–2.39) and the median of the high and low MSANTD3 group was 2.6 and 6.1 years respectively (Fig. 2B). To affirm the prognostic value of MSANTD3 for HNSCC patients, we further conducted the Kaplan-Meier disease-specific survival analysis log-rank test to compare the disease-specific survival of the high and low-risk groups. Results showed that the high MSANTD3 group (50–100%) had a significantly higher overall survival rate than the low MSANTD3 group (0–50%). The hazard ratio of the high group calculated by Cox regression was 2.27 (95%CI = 1.572–3.282) even higher than that of the overall survival (Fig. 2C). As most of the survival records were ended at 5 years, we plotted the data of the first 5 years to clarified the difference between high and low-risk groups. At a higher magnification, the death number was shown by year in Fig. 2D.

Table 1
Patient characteristics in the MSANTD3 high group and MSANTD3 low group (50%)

	MSANTD3 high	MSANTD3 low	P_value
Alive	62	89	
Dead	64	37	0.001
Mean (SD)	61.4 (11.5)	61.5 (12.8)	
Median [MIN-MAX]	61 [26–88]	61 [24–90]	0.923
FEMALE	30	45	
MALE	96	81	0.054
ASIAN	3	3	
BLACK	11	7	
WHITE	108	112	0.618
T1	6	9	
T2	38	31	
T3	30	39	
T4	7	9	
T4a	39	35	
T4b	2	1	
TX	4	2	0.683
N0	59	67	
N1	17	21	
N2	6	4	
N2a	2	5	
N2b	21	16	
N2c	11	8	
N3	4	1	
NX	6	4	0.544
M0	119	122	
M1	1		
MX	6	4	0.737
I	4	11	
II	21	20	
III	20	24	
IVA	78	68	
IVB	3	2	
IVC		1	0.338
G1	3	25	
G2	75	74	
G3	44	25	
GX	3	2	0
Metastasis	5	3	
Primary	1	3	
Recurrence	12	8	0.401

	MSANTD3 high	MSANTD3 low	P_value
Non-smoking	24	35	
Smoking	99	90	0.155
Non-radiation	17	17	
Radiation	31	30	1
Neoadjuvant	3		
No neoadjuvant	123	126	
Chemotherapy	41	35	
Chemotherapy: Targeted Molecular therapy	2	1	
Immunotherapy	1		
Chemotherapy: Immunotherapy	1		1

3.3. The construction of nomogram

To investigate the association of MSANTD3 with other common prognostic factors and further demonstrate the value of MSANTD3 as a prognostic biomarker, we conducted the cox regression analysis for MSANTD3, age, gender, race, pT stage, and pN stage. Univariate Cox regression showed that MSANTD3, age, and pN stage were risk factors for HNSCC patients with a hazard ratio of 1.45, 1.02, and 1.18 respectively (Fig. 3A). Multivariable cox regression analysis revealed that MSANTD3, age, and pN stage were independent factors that affected the overall survival of HNSCC patients (Fig. 3B). Based on the multivariable cox regression analysis, a nomogram was constructed (Fig. 3C). The nomogram aimed for the prediction of 1-, 3-, 5- year survival for HNSCC patients. The nomogram calibration curves showed that the predicted overall survival was consistent with observed survival data (Fig. 3D). The nomogram established a clinical prognostic model of applying MSANTD3 as a biomarker for HNSCC.

3.4. Identification of potential roles of MSANTD3 in HNSCC

To obtain information on the potential mechanisms involved in the effect of the MSANTD3 gene on HNSCC, we first constructed the MSANTD3 associated protein-protein interaction network using the String. The protein-protein interaction network showed the closely interacted proteins of MSANTD3 (Fig. 4A). In addition, we identified differentially expressed genes (DEGs) between MSANTD3 high (75–100%) and low (0–25%) groups. As the differential expression gene analysis aimed to identify differential expression genes in samples with distinctive differences in MSANTD3, we excluded the middle 50% MSANTD3 sample and only analyzed the high 25% samples and low 25% samples. We set the cutoff fold change value of 2 and the p-value of 0.05. Results showed that 242 (up) and 194 (down) genes were identified as DEGs positively and negatively associated with MSANTD3 in HNSCC respectively (Fig. 4B-C). These genes were listed in Table 2. These genes were further enriched in GO terminologies and KEGG pathways. Results of KEGG enrichment showed that genes positively associated with MSANTD3 were enriched in “PI3K − Akt signaling pathway” and “Focal adhesion”, while genes negatively associated with MSANTD3 were enriched in “Staphylococcus aureus infection”, “IL − 17 signaling pathway”, and “Estrogen signaling pathway”. In terms of GO enrichment, genes positively associated with MSANTD3 were enriched in “extracellular structure organization” and “extracellular matrix organization”, while genes negatively associated with MSANTD3 were enriched in “epidermis development”, “skin development”, and “epidermal cell differentiation” (Fig. 4D). Based on these results, we suggested that MSANTD3 might play a role in HNSCC metastasis. However, the intersection analysis of protein-protein interaction (PPI) network genes and differentially expressed genes showed that only one gene, FDCSP, was at the intersection of PPI network genes and negatively associated genes. As the PPI was based on present knowledge of the MSANTD3, these results indicated that most of the potential MSANTD3 associated genes have not been spotted.

Table 2
Differentially expressed genes

Positively associated with MSANTD3 (up)									
PRXL2C	LRRC8C	NRP2	DKK3	BVES	SHANK2	TXNRD1	COL5A3	SLC16A2	CXCL5
P4HA1	WDR54	NRSN2	KIRREL1	MET	GOLIM4	CXCL3	ANO1	WNT7A	COL10A1
ITGA5	OSMR	SLC39A14	PDPN	ITGB1	TINAGL1	C1QTNF6	MMP10	RPL39L	POSTN
TRIM32	CSGALNACT2	LIMA1	CERCAM	TOX2	HAS2	NCEH1	HOXB9	LTBP1	GPC4
IKBIP	GNA12	TNC	CSF2	FSTL3	FADD	TFPI2	AXL	INHBB	MMP1
STC2	FHL2	PLAUR	TPM1	CDH13	CCND1	PTHLH	COL4A6	CA9	IRX4
SERPINE1	CAV2	ANLN	S1PR3	KIAA1549L	DCBLD2	MT2A	FEZ1	CLMP	SLITRK6
STX2	EIF5A2	P4HA2	ARSJ	PANX2	MFAP2	COL4A5	FAT1	TPM2	NEFL
NEK6	ANO6	SPOCK1	LAMC1	ITGA6	CDK6	HMGA2	TENM3	COL12A1	IL24
TGFBR1	CDC42EP3	CALU	CAV1	FERMT2	STC1	NDRG1	SDC2	COL5A2	COL17A1
VAV2	ERFE	FNDC3B	SRPX	FOXM1	ANTXR2	FOXC2	TIMP3	PXDN	MMP7
TNFRSF12A	NT5E	MARVELD1	AMIGO2	EMP3	MICAL2	ICAM1	ITGB6	MMP9	UCHL1
NFIL3	LOXL2	MSC	KDELR3	DSG2	TNFAIP3	TNFAIP6	CTSV	CA12	MMP13
PLAU	FADS3	IL11	PMEPA1	SLC35F3	ITGA3	FAP	GFPT2	MMP12	COL11A1
B4GALNT1	KLF7	TPST1	CAMK2N1	VEGFC	THBS1	GEM	NRG1	SH2D5	AMTN
PLOD3	PDGFA	IL1RAP	LAMA3	APCDD1L	ENO2	FOSL1	SEMA3C	CCNA1	COL3A1
DZIP1L	PDGFB	DKK1	APLN	RAI14	WNT9A	SULF2	IL7R	CACNG4	
LAMC2	TMEM200B	ETV5	PRSS23	SCG5	PPP4R4	ADAMTS15	ACKR3	ADAM12	
CTNNAL1	COL27A1	MMP14	SOX9	L1CAM	SYT7	SGCE	IRX2	SHISA2	
CD276	PDGFC	SLC2A6	FOXL1	ITGAV	FADS1	SPP1	COL5A1	CTHRC1	
SNAI2	CREB5	SERPINH1	PHLDB2	IGF2BP2	FOXD1	SLC12A7	BARX1	SULF1	
PLOD2	LAMB3	DCBLD1	GSDME	CAVIN3	EPHB2	MELTF	CXCL8	NID1	
LGALS1	KIF3C	CDK18	CREG2	MYADM	MSRB3	PPFIA1	P3H2	CDH11	
LARP6	TGFBI	EVA1A	BCAR3	SERPINE2	TMEM158	FN1	TENM2	NUDT11	
POPDC3	ACTN1	INHBA	CTSL	IL6	LIF	ARSI	CORO6	AREG	
Negatively associated with MSANTD3 (down)									
PRSS27	CEACAM7	HAL	FOXN1	GRHL3	SCNN1A	LCE3A	S100A7		
KRT78	A2ML1	CLIC3	ENDOU	PPL	IGLL5	LOR	IL36RN		
CXCL17	TMEM125	SLURP1	TMPRSS11A	WFDC12	DHRS9	PRR9	DSG1		
NCCRP1	MACC1	SPRR2A	SCEL	SLPI	KLK11	CRCT1	PI3		
TM7SF2	KRT4	SPNS2	KLK13	KRT23	RAET1E	CAPNS2	SERPINB4		
CSTB	EPS8L1	TREX2	SERPINB12	IL36A	LY6G6C	CYP4F22	SPRR2G		
GDPD3	RASAL1	S100A8	ANKRD22	SPRR2E	TMEM45B	LCN2	CCL19		
LYPD2	SULT2B1	VSIG8	ALOX12B	EPHX3	S100P	LCE2B	KRT6C		
CYP4B1	CALML5	ASPG	ST6GALNAC1	TMPRSS11B	SERPINB13	SBSN	PRSS3		
FUT6	MUC15	CEACAM6	KLK14	HOPX	ALDH3B2	PDZK1IP1	SPRR4		
FAM3D	ATP10B	AQP3	DYNAP	RDH12	OTOP3	PLA2G4E	SERPINB2		
GGT6	BNIPL	SCNN1B	FAM83C	TGM1	TCN1	KLK6	KRT16		
ANKRD35	C15orf62	S100A9	PSCA	JCHAIN	KRT80	CRISP3	KLK10		
ANXA9	KLK12	SPRR2F	TMPRSS2	KRT2	DUOXA2	SOX21	S100A7A		

Positively associated with MSANTD3 (up)							
SPRR3	SPINK7	TMPRSS11E	SLC26A9	SERPINB11	IVL	KRTDAP	LY6D
CSTA	ATP13A4	CLCA4	SLC6A14	SPRR2D	PGLYRP3	WFDC5	KLK7
SPINK5	TTC9	RHCG	ZNF750	PSORS1C2	DUOX2	SERPINB3	LCE3E
BICDL2	MAL	RNF222	SPRR1A	ASPRV1	CAPN14	KRT1	FDCSP
STX19	VSIG10L	C10orf99	TMPRSS11D	TJP3	FAM3B	DEFB4B	LCE3D
KRT13	DNASE1L3	CD177	MUC20	FAM25A	KRT10	DEFB4A	
CNFN	CYP2C18	RPTN	DEFB1	CALML3	LCE2C	KPRP	
MAB21L4	CYSRT1	ELF5	MZB1	PCP4L1	ZBTB7C	DAPL1	
FUT3	TGM3	MUC21	CD79A	PLA2G4D	SDR9C7	AZGP1	
CRNN	LYNX1	ACER1	CLDN17	SPRR2B	SPRR1B	DMKN	
CEACAM5	RAB25	KRT24	POF1B	S100A12	CDSN	GSDMA	

3.5. MSANTD3 expression difference between metastasis and primary HNSCC.

To further investigate the role of MSANTD3 in HNSCC metastasis, we compared the mRNA expression of MSANTD3 in TCGA M0 and M1 HNSCC samples. However, as there were only five M1 samples, the results showed no significance (Fig. 5A). Thus, we collected cancer tissue samples from 16 patients with primary HNSCC and 16 patients with HNSCC metastasis. We conducted QPCR and western blotting to compare MSANTD3 expression levels in metastasis and primary HNSCC samples. Results showed that metastasis HNSCC samples had a higher level of MSANTD3 at mRNA levels (Fig. 5B). The western blotting further validated that metastasis HNSCC expressed significantly higher MSANTD3 protein compared to the primary HNSCC tissue (Fig. 5C-D). The images of immunohistochemistry staining of MSANTD3 protein in metastasis HNSCC samples also showed a stronger signal than that in primary HNSCC samples (Fig. 5E). Regarding the significance in MSANTD3 between metastasis and primary HNSCC, we proposed that the MSANTD3 molecule might have a direct effect on HNSCC migration.

3.6. The expression of MSANTD3 in HNSCC cell lines.

To test this hypothesis, we designed experiments using HNSCC cell models. We first screened proper cell lines for the study. We plotted the MSANTD3 expression in 33 HNSCC cell lines in the CCLE database. We found that all these 33 cell lines expressed MSANTD3 (Fig. 6A). Then we validated the MSANTD3 levels in eight of these cell lines using QPCR and western blotting in our lab. These eight cell lines included HSC-3, SNU-46, YD-15, YD-38, BIR-16, BICR-22, BICR-6, and BICR-56, which are all commonly used HNSCC cell lines in the field. The QPCR showed that HSC-3 had the highest expression of MSANTD3 mRNA while BICR-22, BICR-6, and BICR-56 had the lowest expression of MSANTD3 mRNA(Fig. 6B). Western blotting results showed a similar trend as the western blotting(Fig. 6C-D).

3.7. Correlation of MSANTD3 expression and HNSCC cell line migration.

Next, we conducted in vitro chemotaxis assay to observe the migration of individual HNSCC cells. The computer recorded the track of the cell every 10 seconds and calculated the velocity of cell migration. Results showed that SNU-46 was the fastest migrating cell line while BICR-56 was the slowest migrating cell line(Fig. 7A-B). We further plotted the correlation of the protein expression of MSANTD3 and the velocity of these eight HNSCC cell lines. Results showed that the protein expression of MSANTD3 is significantly correlated with the velocity of eight HNSCC cell lines with a correlation coefficient of 0.37 (95%CI = 0.18-2.00)(Fig. 7C).

3.8. The knockdown and overexpression of MSANTD3 in YD-15 cells

To investigate whether MSANTD3 was functional in HNSCC migration regulations, we overexpressed MSANTD3 in one of the HNSCC cell lines, YD-15. YD-15 was one of the cell lines that expressed a relatively high level of MSANTD3 and migrated relatively fast. Results showed that 20 nM of MSANTD3 expressing plasmid highly improved the levels of MSANTD3 in YD-15 cells (Fig. 8A-B). The overexpression of MSANTD3 plasmid-concentration-dependently increased the velocity of the migration of YD-15 cells compared to the control from 1 nM to 20 nM (Fig. 8C-D). In addition, we also knocked down MSANTD3 expression in YD-15 cells. The result showed that MSANTD3 shRNA plasmid almost plasmid-concentration-dependently reduced the expression of MSANTD3 in YD-15 cells (Fig. 8E-F). The chemotaxis assay results showed that the knockdown of MSANTD3 significantly reduced the velocity of the migrations of YD-15 cells (Fig. 8G-H). We also plotted the MSANTD3 expression versus velocity of YD-15 migration, generally, the velocity of YD-15 migration was dependent on the expression level of MSANTD3.

3.9. The knockdown and overexpression of MSANTD3 in BICR-56 cells

To affirm the functional effect of MSANTD3 in HNSCC migration, we overexpressed MSANTD3 in another HNSCC cell line, BICR-56, where the MSANTD3 expression was low. Results showed that 20 nM of MSANTD3 expressing plasmid highly improved the levels of MSANTD3 in BICR-56 cells (Fig. 9A-B). The overexpression of MSANTD3 plasmid-concentration-dependently increased the velocity of the migration of BICR-56 cells compared to the control

from 1 nM to 20 nM (Fig. 9C-D). In addition, we also knocked down MSANTD3 expression in BICR-56 cells. The result showed that MSANTD3 shRNA plasmid at 1 nM to 20 nM only slightly reduced the expression of MSANTD3 in BICR-56 cells, which was not plasmid-concentration-dependently (Fig. 9E-F). Plasmid-concentration at 1 to 20 nM has a similar reduction at the MSANTD3 level. Results also showed that the knockdown of MSANTD3 did not significantly reduce the velocity of the migrations of BICR-56 cells (Fig. 9G-H). We also plotted the MSANTD3 expression versus velocity of BICR-56 migration, generally, the velocity of YD-15 migration was dependent on the expression level of MSANTD3.

4. Discussion

This is the first study that demonstrated MSANTD3 was valuable for HNSCC diagnosis and prognosis. On one hand, our analysis indicated that MSANTD3 was overexpressed in HNSCC compared with the normal head and neck tissues. This revealed the potential for using MSANTD3 for HNSCC diagnosis. We also found evidence from open data sets suggesting that the copy number of MSANTD3 in HNSCC was higher than that in normal tissues. We suggested that the higher copy number might account for the higher expression level of MSANTD3 mRNA, yet there might be other factors that can also contribute to the higher expression, such as transcriptional factor and methylations, which required further exploration. On the other hand, as shown in Fig. 2B, the overall survival rate of HNSCC patients was significantly different between MSANTD3 high and MSANTD3 low samples, indicating the association of overall survival and the expression of MSANTD3 in HNSCC tissues. The diagnostic and prognostic potential of MSANTD3 has been reported in other types of cancers. For example, in breast cancer, MSANTD3 was found overexpressed in cancer tissue than adjacent normal breast tissues [7]. In non-small cell lung cancer, MSANTD3 was also identified as a biomarker that potentially affects therapeutic response in patients [8]. In Fig. 3, high expression of MSANTD3 was associated with a worse prognosis and the prognosis of MSANTD3 was independent of age and pN stage. All these bioinformatic studies demonstrated the potential clinical value of MSANTD3 as a prognosis biomarker.

One of the most significant findings of this study was that we are the first study to report that MSANTD3 might increase HNSCC cell migration. The previous studies only reported the functional roles of MSANTD3 inside cells[5, 9], but little is known about its role in cell-cell interactions. Our DEGs enrichment study inferred a potential association of MSANTD3 and the regulation of the extracellular matrix, which is critical in cell migration and cancer metastasis. It has been reported that once HNSCC patients present with recurrence and/or metastasis, the median overall survival (OS) hardly exceeds 12 months [17], thus the migration of HNSCC cells has been one of the most concerns for HNSCC study. In this study, we collected clinical samples of metastasis HNSCC and primary HNSCC and compared the expression of MSANTD3. A commonly used QPCR and western blotting assay were conducted [18, 19], which suggested that MSANTD3 was overexpressed in the metastasis samples compared to primary samples.

One of the special of our study was we determined multiple cell lines. The correlation of HSCN1 expression and velocity of migration of the eight HNSCC cell lines we tested strongly suggested that MSANTD3 was a regulatory molecule for HNSCC cell migration. We validated the promoting effect of MSANTD3 on HNSCC cell migration by overexpressing MSANTD3 in YD-15 cells. These results were consistent with our hypothesis that MSANTD3 regulated cancer cell migration and metastasis. Furthermore, most of the previous studies investigated cancer cell migration using the wound-healing or the transwell assay [20], which determined the migration of a group of cancer cells as a whole. Our study was the first to investigate the role of MSANTD3 by tracking individual cell migration. Nevertheless, although we obtain the velocity of individual cell migration, we were not able to determine the expression of MSANTD3 in the cell we recorded. In addition, cancer cells might have different manners under in vivo or in-vitro conditions. Animal models have been widely used in research [21–23]. Further study should apply the in vivo orthotopic xenografts mice model to verify the role of MSANTD3 in HNSCC cell invasion and metastasis.

The potential regulation of MSANTD3 on cancer migration might contribute to the effects of these factors on cancers. Yet, further studies are required to identify the direct impact of MSANTD3 on cancer cell migration. This study aimed to validate the role of MSANTD3 in HNSCC cell migration, but the limitation of the study is that we only provided evidence supporting the functional effect of MSANTD3 on cancer cell migration, yet, the mechanisms underlying these effects were not clear. The enrichment analysis revealed several potential mechanisms, such as the PI3K − Akt signaling pathway, IL − 17 signaling pathway, and Estrogen signaling pathway, that required further validation with experimental evidence. In addition, as the enrichment data revealed that MSANTD3 might associate with the PI3K − Akt signaling pathway, which is the ion-homeostasis associated pathway[24, 25], many cancer-related ion channels, such as VGSC[26–28], TRP[29, 30], and TPCs[31, 32] might be involved. The role of most of these ion channels remains unclear and whether they contribute to the effects of MSANTD3 on cancer cells needs further investigation. In the clinical treatment of human disease, many different therapies might be applied[33]. In cancer treatment, many drugs might directly or indirectly affect cancer metastasis by either regulated cancer cells or the immune system such as the use of anesthetics or traditional medicines [20, 34–40]. We think MSANTD3 can be a drug target candidate for general cancer but not only HNSCC.

In conclusion, this is the first study with HNSCC and MSANTD3. We demonstrated that 1) MSANTD3 is higher expressed in HNSCC than normal tissue and in metastatic than primary tumor; 2) cells with high MSANTD3 presented higher migration velocity; 3) the overexpression and knockdown of MSANTD3 interfered on cell migration; 4) further study should apply the in vivo orthotopic xenografts mice model to verify the role of MSANTD3 in HNSCC cell invasion and metastasis.

Declarations

Ethics approval and consent to participate

The study has been approved by the Ethics Committee of Hainan General Hospital (2022-11) following the Helsinki Declaration. All methods were carried out in accordance with relevant guidelines and regulations. Informed consent was obtained from all subjects.

Consent for publication

All the authors have given consent for publication.

Availability of data and materials

Data are available from the corresponding author for a reasonable request.

Competing interests

The authors claimed that there is no conflict of interest.

Funding

This study was supported by the Natural Science Foundation of Hainan Province (No. 818QN311).

Authors' contributions

INTERPRETATION OR ANALYSIS OF DATA: Yuliang Zhang and Jiabin Nian

PREPARATION OF THE MANUSCRIPT: Anyan Zhou and Jing Zheng

REVISION FOR IMPORTANT INTELLECTUAL CONTENT: Shuzhou Liu

SUPERVISION: Shuzhou Liu

Acknowledgments

We thank the support of Hainan Affiliated Hospital of Hainan Medical University.

References

1. Siegel, R.L.; Miller, K.D.; Jemal, A. Cancer statistics, 2019. *CA Cancer J Clin***2019**, *69*, 7-34, doi:10.3322/caac.21551.
2. Miller, K.D.; Nogueira, L.; Mariotto, A.B.; Rowland, J.H.; Yabroff, K.R.; Alfano, C.M.; Jemal, A.; Kramer, J.L.; Siegel, R.L. Cancer treatment and survivorship statistics, 2019. *CA Cancer J Clin***2019**, *69*, 363-385, doi:10.3322/caac.21565.
3. Johnson, D.E.; Burtness, B.; Leemans, C.R.; Lui, V.W.Y.; Bauman, J.E.; Grandis, J.R. Head and neck squamous cell carcinoma. *Nature Reviews Disease Primers***2020**, *6*, 92, doi:10.1038/s41572-020-00224-3.
4. Duprez, F.; Berwouts, D.; De Neve, W.; Bonte, K.; Boterberg, T.; Deron, P.; Huvenne, W.; Rottey, S.; Mareel, M. Distant metastases in head and neck cancer. *Head & neck***2017**, *39*, 1733-1743, doi:10.1002/hed.24687.
5. Barasch, N.; Gong, X.; Kwei, K.A.; Varma, S.; Biscocho, J.; Qu, K.; Xiao, N.; Lipsick, J.S.; Pelham, R.J.; West, R.B., et al. Recurrent rearrangements of the Myb/SANT-like DNA-binding domain containing 3 gene (MSANTD3) in salivary gland acinic cell carcinoma. *PLoS One***2017**, *12*, e0171265, doi:10.1371/journal.pone.0171265.
6. Lee, D.Y.; Brayer, K.J.; Mitani, Y.; Burns, E.A.; Rao, P.H.; Bell, D.; Williams, M.D.; Ferrarotto, R.; Pytynia, K.B.; El-Naggar, A.K., et al. Oncogenic Orphan Nuclear Receptor NR4A3 Interacts and Cooperates with MYB in Acinic Cell Carcinoma. *Cancers***2020**, *12*, doi:10.3390/cancers12092433.
7. Song, Q.; Jing, H.; Wu, H.; Zhou, G.; Kajiyama, T.; Kambara, H. Gene expression analysis on a photodiode array-based bioluminescence analyzer by using sensitivity-improved SRPP. *The Analyst***2010**, *135*, 1315-1319, doi:10.1039/c0an00012d.
8. Mohammed Ael, S.; Eguchi, H.; Wada, S.; Koyama, N.; Shimizu, M.; Otani, K.; Ohtaki, M.; Tanimoto, K.; Hiyama, K.; Gaber, M.S., et al. TMEM158 and FBLP1 as novel marker genes of cisplatin sensitivity in non-small cell lung cancer cells. *Experimental lung research***2012**, *38*, 463-474, doi:10.3109/01902148.2012.731625.
9. Andreasen, S.; Varma, S.; Barasch, N.; Thompson, L.D.R.; Miettinen, M.; Rooper, L.; Stelow, E.B.; Agander, T.K.; Seethala, R.R.; Chiosea, S.I., et al. The HTN3-MSANTD3 Fusion Gene Defines a Subset of Acinic Cell Carcinoma of the Salivary Gland. *The American journal of surgical pathology***2019**, *43*, 489-496, doi:10.1097/pas.0000000000001200.
10. Rhodes, D.R.; Yu, J.; Shanker, K.; Deshpande, N.; Varambally, R.; Ghosh, D.; Barrette, T.; Pandey, A.; Chinnaiyan, A.M. ONCOMINE: a cancer microarray database and integrated data-mining platform. *Neoplasia (New York, N.Y.)***2004**, *6*, 1-6, doi:10.1016/s1476-5586(04)80047-2.
11. Peng, C.H.; Liao, C.T.; Peng, S.C.; Chen, Y.J.; Cheng, A.J.; Juang, J.L.; Tsai, C.Y.; Chen, T.C.; Chuang, Y.J.; Tang, C.Y., et al. A novel molecular signature identified by systems genetics approach predicts prognosis in oral squamous cell carcinoma. *PLoS One***2011**, *6*, e23452, doi:10.1371/journal.pone.0023452.
12. Ye, H.; Yu, T.; Temam, S.; Ziober, B.L.; Wang, J.; Schwartz, J.L.; Mao, L.; Wong, D.T.; Zhou, X. Transcriptomic dissection of tongue squamous cell carcinoma. *BMC genomics***2008**, *9*, 69, doi:10.1186/1471-2164-9-69.
13. Szklarczyk, D.; Morris, J.H.; Cook, H.; Kuhn, M.; Wyder, S.; Simonovic, M.; Santos, A.; Doncheva, N.T.; Roth, A.; Bork, P., et al. The STRING database in 2017: quality-controlled protein-protein association networks, made broadly accessible. *Nucleic Acids Res***2017**, *45*, D362-d368,

doi:10.1093/nar/gkw937.

14. Li, X.; Peng, B.; Zhu, X.; Wang, P.; Xiong, Y.; Liu, H.; Sun, K.; Wang, H.; Ou, L.; Wu, Z., et al. Changes in related circular RNAs following ERbeta knockdown and the relationship to rBMSC osteogenesis. *Biochemical and biophysical research communications***2017**, *493*, 100-107, doi:10.1016/j.bbrc.2017.09.068.
15. Pepperell, E.E.; Watt, S.M. A novel application for a 3-dimensional timelapse assay that distinguishes chemotactic from chemokinetic responses of hematopoietic CD133(+) stem/progenitor cells. *Stem cell research***2013**, *11*, 707-720, doi:10.1016/j.scr.2013.04.006.
16. Zantl, R.; Horn, E. Chemotaxis of slow migrating mammalian cells analysed by video microscopy. *Methods in molecular biology (Clifton, N.J.)***2011**, *769*, 191-203, doi:10.1007/978-1-61779-207-6_13.
17. Saada-Bouzid, E.; Peyrade, F.; Guigay, J. Molecular genetics of head and neck squamous cell carcinoma. *Current opinion in oncology***2019**, *31*, 131-137, doi:10.1097/cco.0000000000000536.
18. Liu, H.; Xiong, Y.; Zhu, X.; Gao, H.; Yin, S.; Wang, J.; Chen, G.; Wang, C.; Xiang, L.; Wang, P., et al. Icariin improves osteoporosis, inhibits the expression of PPARgamma, C/EBPalpha, FABP4 mRNA, N1ICD and jagged1 proteins, and increases Notch2 mRNA in ovariectomized rats. *Experimental and therapeutic medicine***2017**, *13*, 1360-1368, doi:10.3892/etm.2017.4128.
19. Liu, X.; Liu, H.; Xiong, Y.; Yang, L.; Wang, C.; Zhang, R.; Zhu, X. Postmenopausal osteoporosis is associated with the regulation of SP, CGRP, VIP, and NPY. *Biomedicine & pharmacotherapy = Biomedecine & pharmacotherapie***2018**, *104*, 742-750, doi:10.1016/j.biopha.2018.04.044.
20. Liu, H.; Dilger, J.P.; Lin, J. Effects of local anesthetics on cancer cells. *Pharmacology & Therapeutics***2020**, *212*, 107558, doi:10.1016/j.pharmthera.2020.107558.
21. Chen, G.; Wang, C.; Wang, J.; Yin, S.; Gao, H.; Xiang, L.U.; Liu, H.; Xiong, Y.; Wang, P.; Zhu, X., et al. Antiosteoporotic effect of icariin in ovariectomized rats is mediated via the Wnt/beta-catenin pathway. *Experimental and therapeutic medicine***2016**, *12*, 279-287, doi:10.3892/etm.2016.3333.
22. Wang, C.; Chen, G.; Wang, J.; Liu, H.; Xiong, Y.; Wang, P.; Yang, L.; Zhu, X.; Zhang, R. Effect of Herba Epimedium Extract on Bone Mineral Density and Microstructure in Ovariectomised Rat. *Journal of Pharmaceutical and Biomedical Sciences***2016**, *6*.
23. Liu, H.; Xiong, Y.; Gao, H.; Yin, S.; Wang, J.; Chen, G.; Wang, C.; Xiang, L.; Wang, P.; Fang, J. Icariin improves osteoporosis, inhibits the expression of PPAR gamma, C/EBP gamma, FABP4 mRNA, N1ICD, and jagged1 proteins and increases Notch2 mRNA in ovariectomized rats. In Proceedings of International journal of molecular medicine; pp. S77-S77.
24. Huang, C.Y.; Hsiao, J.K.; Lu, Y.Z.; Lee, T.C.; Yu, L.C. Anti-apoptotic PI3K/Akt signaling by sodium/glucose transporter 1 reduces epithelial barrier damage and bacterial translocation in intestinal ischemia. *Laboratory investigation; a journal of technical methods and pathology***2011**, *91*, 294-309, doi:10.1038/labinvest.2010.177.
25. Divolis, G.; Mavroeidi, P.; Mavrofrydi, O.; Papazafiri, P. Differential effects of calcium on PI3K-Akt and HIF-1α survival pathways. *Cell Biology and Toxicology***2016**, *32*, 437-449, doi:10.1007/s10565-016-9345-x.
26. Liu, H. Nav channels in cancers: Nonclassical roles. *Global Journal of Cancer Therapy***2020**, *6*, 5, doi:https://dx.doi.org/10.17352/gjct.
27. House, C.D.; Vaske, C.J.; Schwartz, A.M.; Obias, V.; Frank, B.; Luu, T.; Sarvazyan, N.; Irby, R.; Strausberg, R.L.; Hales, T.G., et al. Voltage-gated Na+ channel SCN5A is a key regulator of a gene transcriptional network that controls colon cancer invasion. *Cancer Res***2010**, *70*, 6957-6967, doi:10.1158/0008-5472.can-10-1169.
28. House, C.D.; Wang, B.D.; Ceniccola, K.; Williams, R.; Simaan, M.; Olender, J.; Patel, V.; Baptista-Hon, D.T.; Annunziata, C.M.; Gutkind, J.S., et al. Voltage-gated Na+ Channel Activity Increases Colon Cancer Transcriptional Activity and Invasion Via Persistent MAPK Signaling. *Sci Rep***2015**, *5*, 11541, doi:10.1038/srep11541.
29. Liu, H.; Dilger, J.P.; Lin, J. The Role of Transient Receptor Potential Melastatin 7 (TRPM7) in Cell Viability: A Potential Target to Suppress Breast Cancer Cell Cycle. *Cancers***2020**, *12*, doi:10.3390/cancers12010131.
30. Liu, H.; Dilger, J.P.; Lin, J. Lidocaine Suppresses Viability and Migration of Human Breast Cancer Cells: TRPM7 as A Target for Some Breast Cancer Cell Lines. *Cancers***2021**, *13*, 234, doi:10.3390/cancers13020234.
31. Liu, H. A prospective for the role of two-pore channels in breast cancer cells. *Global Journal of Cancer Therapy***2020**, *6*, 001–003, doi:10.17352/2581-5407.000026.
32. Chen, C.C.; Krogsaeter, E.; Grimm, C. Two-pore and TRP cation channels in endolysosomal osmo-/mechanosensation and volume regulation. *Biochimica et biophysica acta. Molecular cell research***2021**, *1868*, 118921, doi:10.1016/j.bbamcr.2020.118921.
33. Haixia, W.; Shu, M.; Li, Y.; Panpan, W.; Kehuan, S.; Yingquan, X.; Hengrui, L.; Xiaoguang, L.; Zhidi, W.; Ling, O. Effectiveness associated with different therapies for senile osteopo-rosis: a network Meta-analysis. *J Tradit Chin Med***2020**, *40*, 17-27.
34. Liu, H. A Prospective for the Potential Effect of Local Anesthetics on Stem-Like Cells in Colon Cancer. *Biomedical Journal of Scientific & Technical Research***2020**, *25*, 18927-18930.
35. Li, R.; Huang, Y.; Liu, H.; Dilger, J.P.; Lin, J. Comparing volatile and intravenous anesthetics in a mouse model of breast cancer metastasis. p. 2162.
36. Li, R.; Liu, H.; Dilger, J.P.; Lin, J. Effect of Propofol on breast Cancer cell, the immune system, and patient outcome. *BMC anesthesiology***2018**, *18*, 77, doi:10.1186/s12871-018-0543-3.
37. Li, R.; Xiao, C.; Liu, H.; Huang, Y.; Dilger, J.P.; Lin, J. Effects of local anesthetics on breast cancer cell viability and migration. *BMC cancer***2018**, *18*, 666.
38. Liu, H. A clinical mini-review: Clinical use of Local anesthetics in cancer surgeries. *The Gazette of Medical Sciences***2020**, *1*, 030-034.
39. Liu, H. Effect of Traditional Medicine on Clinical Cancer. *Biomedical Journal of Scientific & Technical Research***2020**, *30*, 23548-23551.

40. Jin, Z.; Zhang, W.; Liu, H.; Ding, A.; Lin, Y.; Wu, S.X.; Lin, J. Potential Therapeutic Application of Local Anesthetics in Cancer Treatment. *Recent patents on anti-cancer drug discovery***2022**, 10.2174/1574892817666220119121204, doi:10.2174/1574892817666220119121204.

Figures

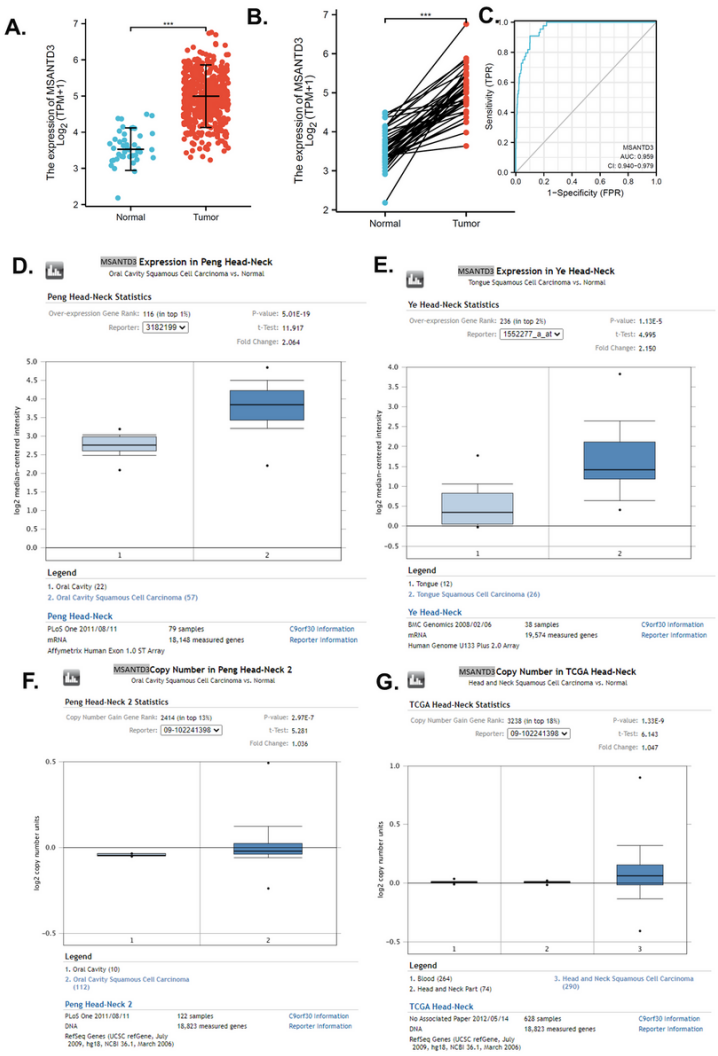

Figure 1

The overexpression of MSANTD3 in HNSCC. A. The expression level of MSANTD3 gene in HNSCC and normal head and neck tissue from TCGA HNSCC dataset (normal n=44, cancer n=502). B. Patient paired cancer-non-cancer comparison of the expression level of MSANTD3 gene in tissue from TCGA HNSCC dataset (n=43). (***p<0.001) C. Receiver operating characteristic (ROC) curve of MSANTD3 HNSCC diagnosis. D-E External validation of MSANTD3 overexpression in HNSCC from Peng's data set (GSE25099) [11] and Ye's data set (GSE9844) [12]. The copy number of MSANTD3 gene in HNSCC and normal head and neck tissue from TCGA data set and Peng's data (GSE25103) [11].

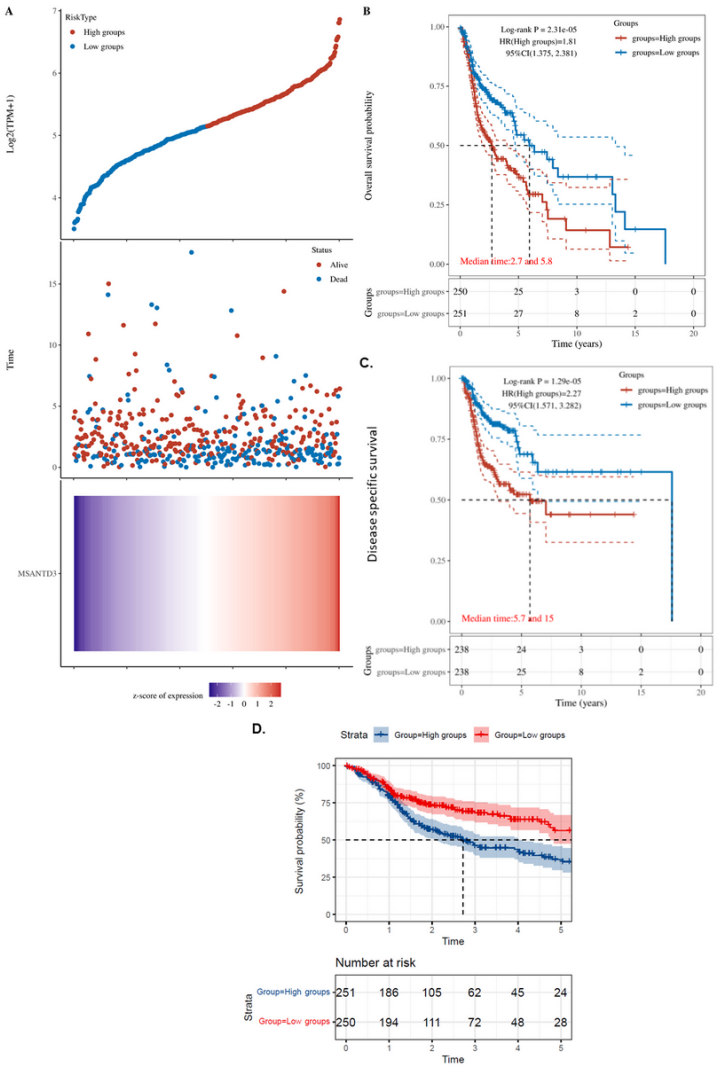

Figure 2

Prognostic power of MSANTD3. A. The curve of MSANTD3 overall survival risk score. Top panel: The dotted line represented the quartile risk score and divided the patients into high and low-risk groups with a cut-off of 50% expression. Middle panel: survival status of the patients. Bottom panel: Heatmap of the expression profiles of MSANTD3. Each point at the top panel and middle panel was vertically corresponding to the z-score of MSANTD3 in each sample at the bottom panel. B. Kaplan-Meier overall survival analysis of the high and low-risk groups. C. Kaplan-Meier disease-specific survival analysis of the high and low-risk groups. The log-rank test p-value and hazard ratio with 95%CI (calculated by Cox proportional hazards regression assuming high and low-risk groups as the category) were shown at the top left. The median survival times were shown at the bottom left. D. Kaplan-Meier's overall survival analysis of the high and low-risk groups of the first 5 years.

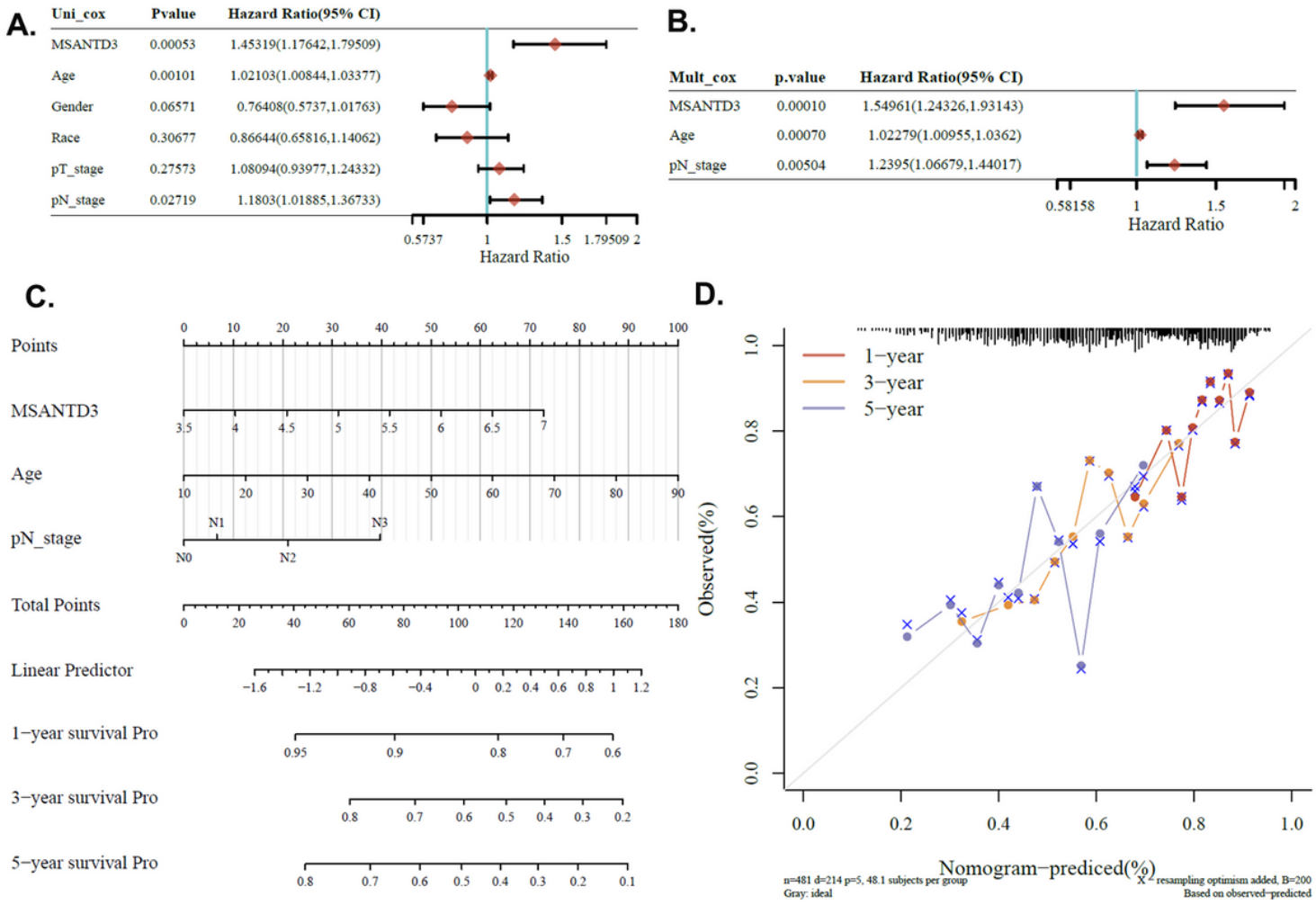

Figure 3

The construction of the nomogram. A. Univariate cox regression analysis of MSANTD3 expression and common clinical factors. B. multivariable cox regression analysis of MSANTD3 expression and common clinical factors. C. Nomogram constructed according to the multivariable regression analysis. D. Calibration curve of the nomogram.

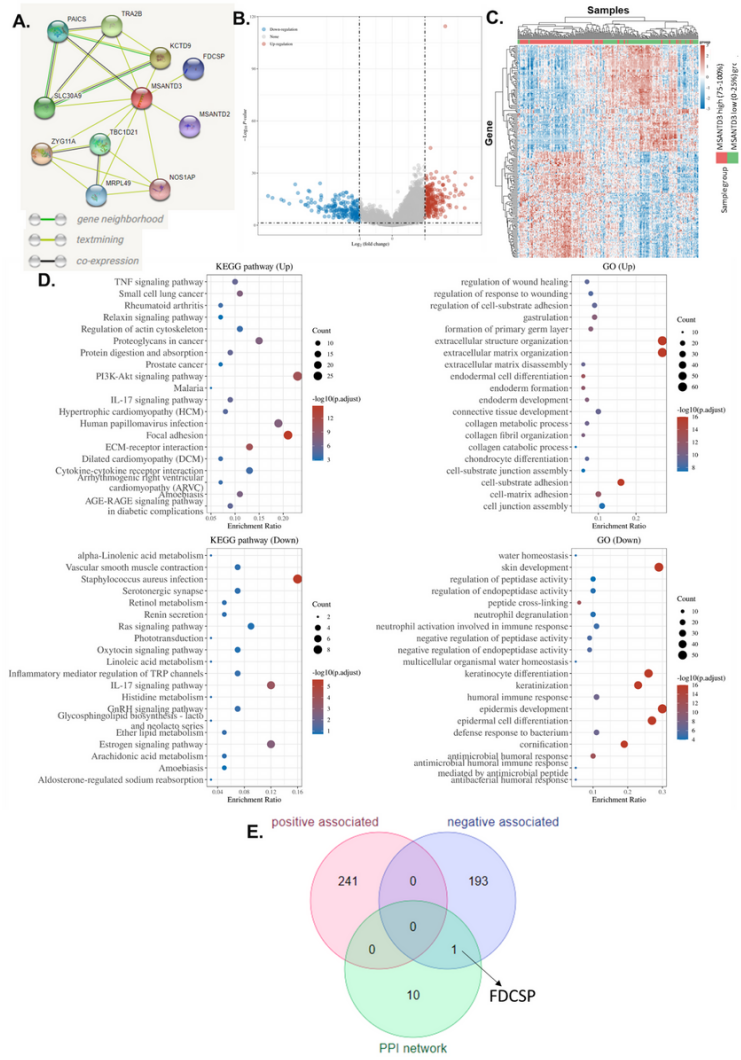

Figure 4

Potential roles of MSANTD3 in HNSCC. A. Construction of MSANTD3 associated protein-protein interaction network. B. Volcano plot of the differentially expressed genes in HNSCC MSANTD3 high (75-100%) and low (0-25%) groups (fold-change >2 and P<0.01). C. Heatmap of the differentially expressed gene in HNSCC MSANTD3 high (75-100%) and low (0-25%) groups. D. The GO and the KEGG signaling pathways enrichment analysis of MSANTD3 associated differentially expressed genes. E. The intersection of protein-protein interaction (PPI) network genes and differentially expressed genes.

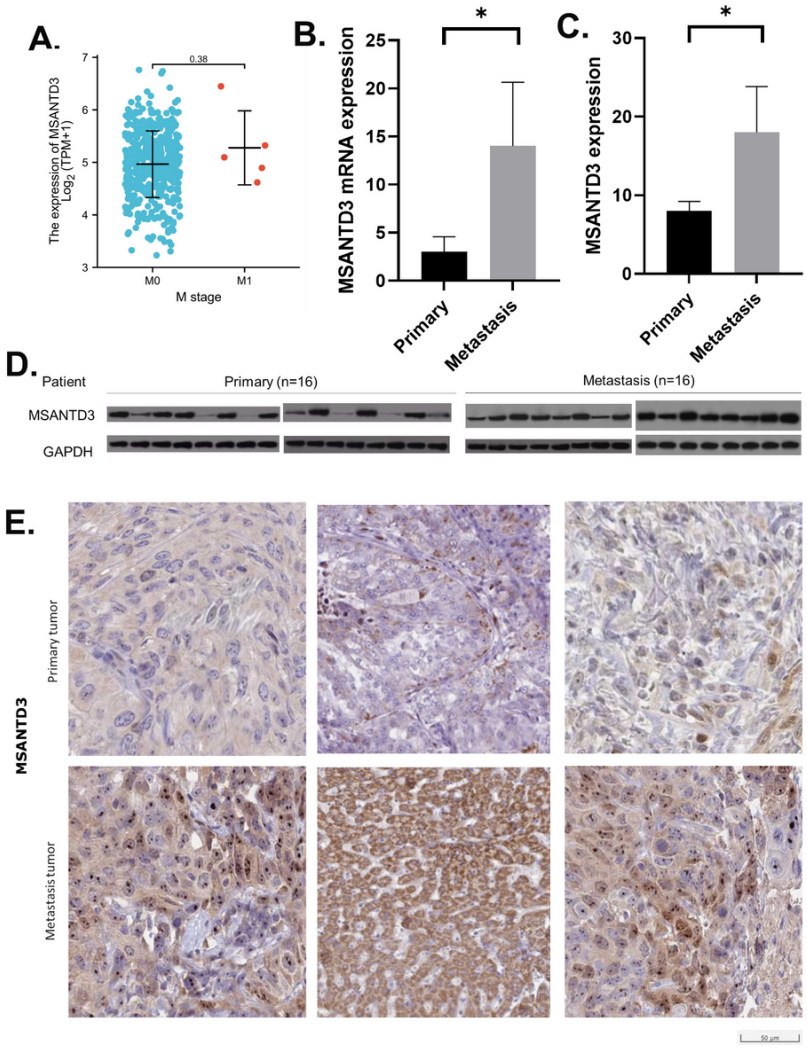

Figure 5

MSANTD3 expression difference between metastasis and primary HNSCC. A. The mRNA expression of MSANTD3 in TCGA M0 (n=472) and M1 (n=5) HNSCC samples. B. The mRNA expression of MSANTD3 in metastasis (n=16) and primary (n=16) HNSCC samples (QPCR). C. The protein expression of MSANTD3 in metastasis (n=16) and primary (n=16) HNSCC samples (western blotting). D. Image of the western blotting. E. Representative image of immunohistochemistry staining of MSANTD3 protein in primary and metastasis HNSCC samples. (*p<0.05)

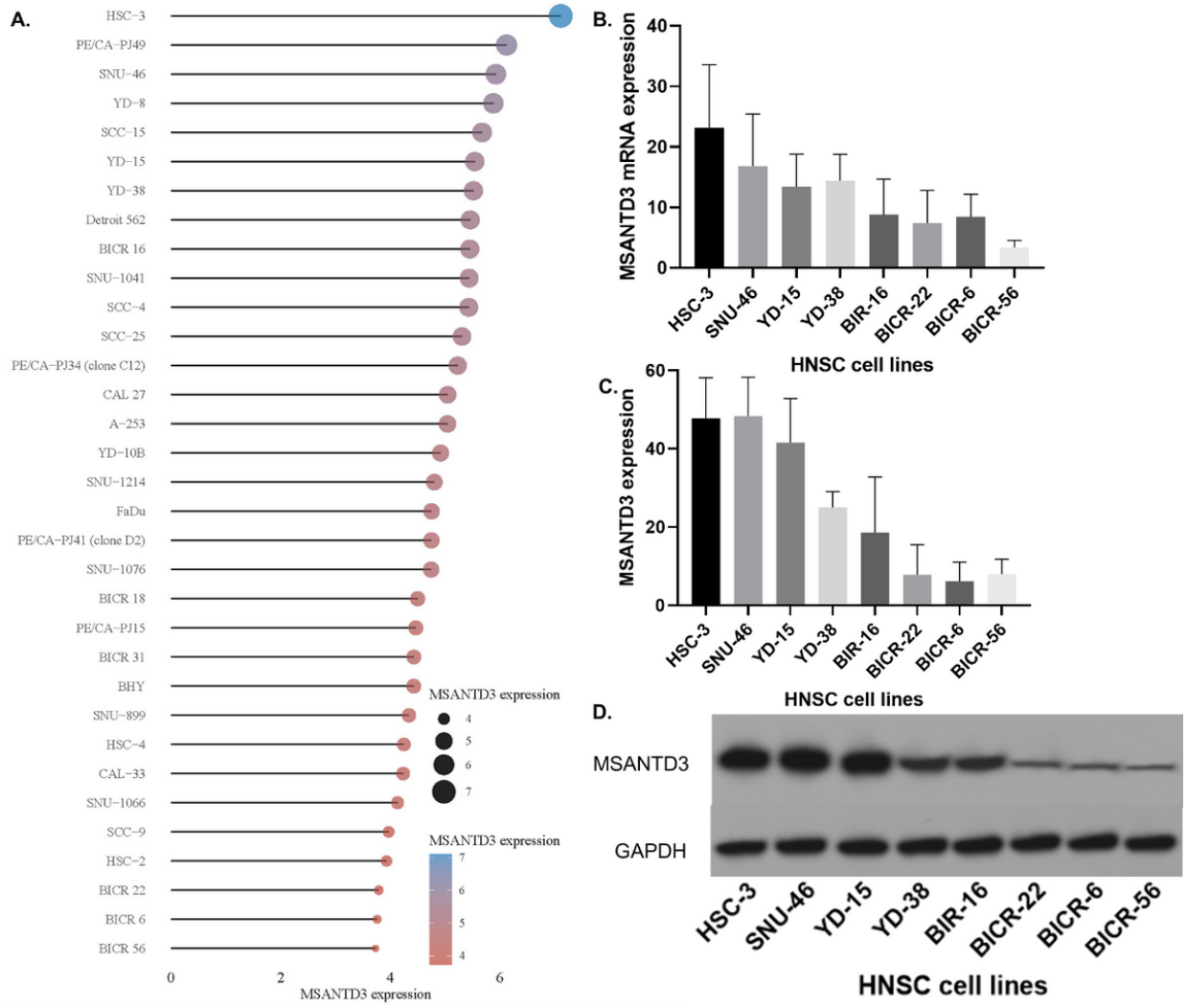

Figure 6

The expression of MSANTD3 in HNSCC cell lines. A. The expression level of MSANTD3 gene in HNSCC cell lines from CCLE dataset. B. The mRNA expression of MSANTD3 in eight HNSCC cell line samples (QPCR). C. The protein expression of MSANTD3 in eight HNSCC cell lines samples (western blotting). D. Image of the western blotting.

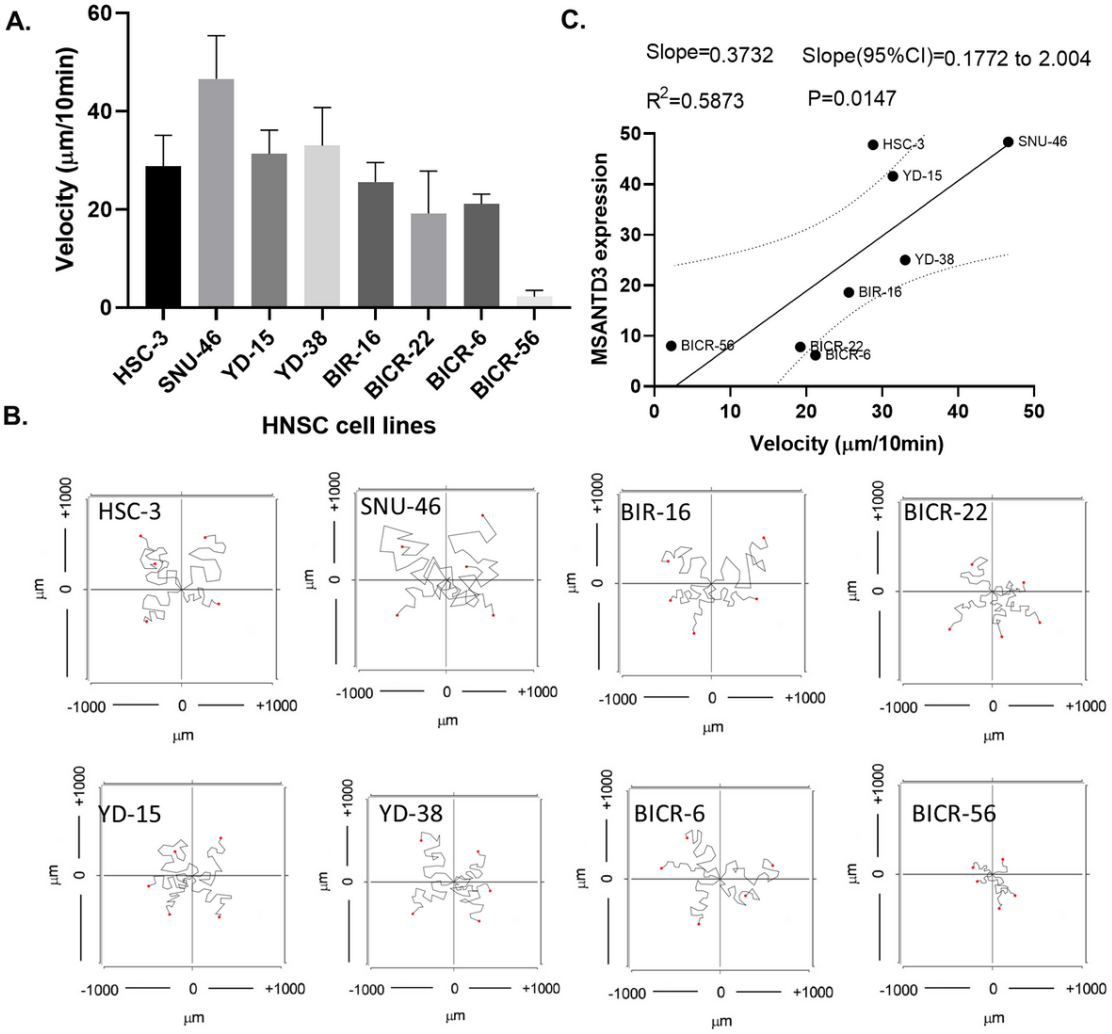

Figure 7

Correlation of MSANTD3 expression and HNSCC cell line migration (n=5). A. The velocity of eight HNSCC cell lines. B. Images of the single-cell migration track. C. Correlation of the protein expression of MSANTD3 and the velocity of eight HNSCC cell lines.

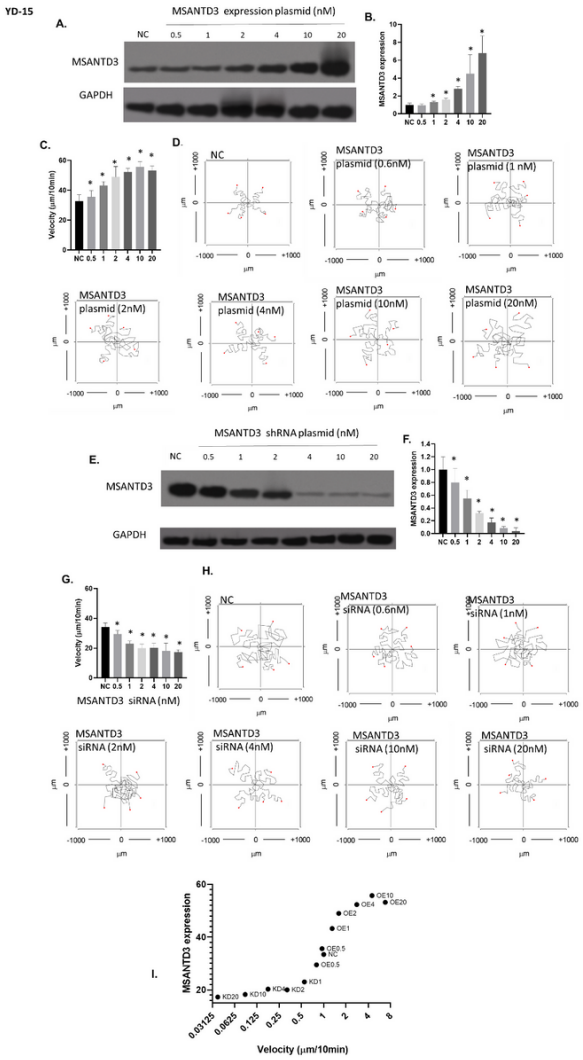

Figure 8

The overexpression and knockdown of MSANTD3 in YD-15 cells. A-B. The protein expression of MSANTD3 in YD-15 cells with different levels of MSANTD3 overexpression. C-D. The velocity of YD-15 cells with or without MSANTD3 overexpression(n=5). E-F. The protein knockdown of MSANTD3 in YD-15 cells with different levels of MSANTD3 overexpression. G-H. The velocity of YD-15 cells with or without MSANTD3 knockdown(n=5). I. Correlation of the protein expression of MSANTD3 and the velocity of YD-15 cells in the overexpression and knockdown experiments. (*p<0.05)

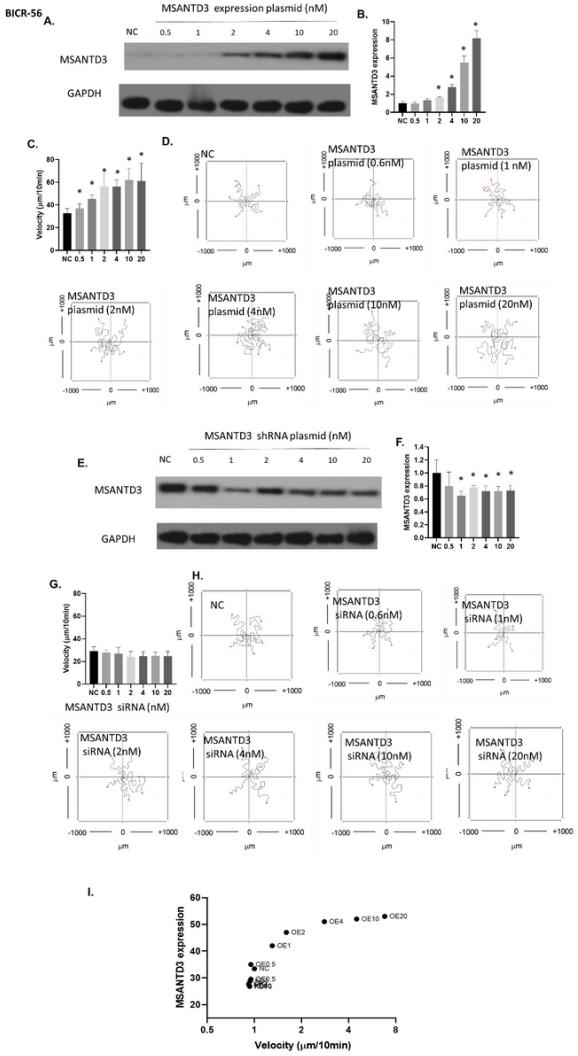

Figure 9

The overexpression and knockdown of MSANTD3 in BICR-56 cells. A-B. The protein expression of MSANTD3 in BICR-56 cells with different levels of MSANTD3 overexpression. C-D. The velocity of BICR-56 cells with or without MSANTD3 overexpression(n=5). E-F. The protein knockdown of MSANTD3 in BICR-56 cells with different levels of MSANTD3 overexpression. G-H. The velocity of BICR-56 cells with or without MSANTD3 knockdown(n=5). I. Correlation of the protein expression of MSANTD3 and the velocity of BICR-56 cells in the overexpression and knockdown experiments. (*p<0.05)

Supplementary Files

This is a list of supplementary files associated with this preprint. Click to download.

- supplimentaryfile.csv
- western.rar